Available online at www.sciencedirect.com

SciVerse ScienceDirect

Ceramics International 39 (2013) 7727–7733

CERAMICS INTERNATIONAL

www.elsevier.com/locate/ceramint

Characterization by Fourier transform infrared spectroscopy of hydroxyapatite co-doped with zinc and fluoride

I. Uysal[a], F. Severcan[a,b], Z. Evis[a,c,*]

[a]Middle East Technical University, Department of Biomedical Engineering, Ankara 06800, Turkey
[b]Middle East Technical University, Department of Biological Sciences, Ankara 06800, Turkey
[c]Middle East Technical University, Department of Engineering Sciences, Ankara 06800, Turkey

Received 16 December 2012; received in revised form 6 March 2013; accepted 10 March 2013
Available online 16 March 2013

Abstract

Pure and Zn^{2+} and/or F^- doped hydroxyapatite (HA) were synthesized by the precipitation method and detection of ion incorporations into the HA structure was investigated by a non invasive Fourier transform infrared (FTIR) spectroscopic technique. The synthesized materials were sintered at 1100 °C for 1 h. The Zn^{2+} addition amount was kept constant at 2 mol% whereas F^- amount was changed. The weight fractions of the HA and CaO were calculated by Rietveld analysis by using GSAS. Co-doping of Zn^{2+} and F^- ions increased the stability of HA. A detailed analysis of FTIR spectroscopy was performed to observe whether HA structure was formed or not. The bands corresponding to the (PO_4^{3-}) functional group and (OH^-) functional group were observed. Moreover, the ion incorporation into the HA structure and the amount of the ions were analyzed by FTIR spectroscopy. The OH…F bands were observed at 711 cm^{-1} and 3543 cm^{-1}. The Zn–O stretching band was observed at 3403 cm^{-1} and 433 cm^{-1}. The area calculation under the OH…F bands and (OH^-) stretching and librational modes of the bands revealed that as the F^- amount increased, the area under the bands at 711 cm^{-1} and 3543 cm^{-1} increased whereas the area under the (OH^-) stretching and librational modes of the bands decreased due to the fact that F^- ion replaced with (OH^-) ion in HA structure. All these results showed that Zn^{2+} and F^- ions were successfully incorporated into the HA structure. Moreover, the amount of F^- ions in the HA structure was successfully confirmed by determination of the area under the F^- and (OH^-) related bands.

Keywords: Infrared spectroscopy; Bioceramics; Chemical synthesis; Microstructure

1. Introduction

Hydroxylapatite (HA) has the chemical formula $Ca_{10}(PO_4)_6(OH)_2$. It has the Ca/P ratio of 1.67. It is a ceramic material and similar to bone mineral in terms of structural and mechanical properties [1]. HA has a structure that enables some ion incorporations. These ion incorporations result in changes in its mechanical and biological properties. Among these ions, K^+, Na^+, Mn^{2+}, Ni^{2+}, Cu^{2+}, Co^{2+}, Sr^{2+}, Ba^{2+}, Pb^{2+}, Cd^{2+}, Y^{3+}, La^{3+}, Fe^{2+}, Zn^{2+}, Mg^{2+}, Ce^{3+}, Al^{3+} can substitute with Ca^{2+} ion. As, P, Si, V, Cr, (CO_3^{2-}) can substitute with (PO_4^{3-}) ion and F^-, Cl^-, O^{2-}, OH^-, Br^- can substitute with (OH^-) ion [2–4]. A study reported that doping of Zn^{2+} ions into HA (with an amount of between 0.6 and 1.2 wt%) helped cell proliferation [5]. Addition of Zn^{2+} increases the alkaline phosphatase activity which is an indicator of cell functionality [6].

Addition of F^- decreases the solubility of the HA and increases its density after the sintering. The increase in density results in improvement in strength and hardness by two or four fold with respect to pure HA [7]. Moreover, crystallinity is improved by addition of F^-. Therefore, it is being used in osteoporosis therapy [7–9]. Furthermore, F^- doped HA increases the collagen synthesis and alkaline phosphatase activity thus affects the cell proliferation indirectly.

FTIR spectroscopic technique is applied to HA to detect the specific bands in HA structure. These bands correspond to the

*Corresponding author at: Middle East Technical University, Department of Engineering Sciences, 06800 Ankara, Turkey. Tel.: +90 312 2104450; fax: +90 312 2104462.
E-mail address: evis@metu.edu.tr (Z. Evis).

0272-8842/$ - see front matter © 2013 Elsevier Ltd and Techna Group S.r.l. All rights reserved.
http://dx.doi.org/10.1016/j.ceramint.2013.03.029

(PO_4^{3-}) functional group with four different vibrational modes (ν_1, ν_2, ν_3, ν_4) and (OH^-) functional group with two different vibrational modes (librational and stretching) [10–12]. The detection of these two functional groups is the indicator of formation of HA structure. Besides these two functional groups, in some previous studies, the bands related to the residual compounds such as (CO_3^{2-}) [13,14], H_2O [14], (NO_3^-) and (NH_4^+) [14,15] were observed. However, when the samples were calcined at 900 °C for 2 h, the bands related to H_2O, (CO_3^{2-}), (NO_3^-) and (NH_4^+) disappeared [15].

FTIR studies of the doped HA samples were also performed. Additional peaks were observed according to the type of bond and type of ion. Kim et al. investigated the effect of F^- ion on HA and alumina composites and FTIR analysis was done for them [16]. Moreover, in a study, 50 mol% F^- substituted HA and pure HA were synthesized by precipitation method and sintered at 1100 °C for 3 h [11]. According to FTIR results, dried samples had a spectra like partially carbonated hydrated HA [11]. Moreover, the F^- doped sample did not show any of (OH^-) peaks [11]. However, an additional peak was observed for fluoridated samples [11]. Fluoride addition also resulted in a shift towards the lower wavenumbers in (OH^-) stretching peak. As the F^- amount increased in the samples, the intensity of the bands related to F^- binding increased, whereas the intensity of the band corresponding to the (OH^-) librational band decreased [11,12]. In another study, fluoridated HA was synthesized by a sol–gel method. After synthesis, heat treatment was applied to the samples at 850 °C for 3 h [17]. It was stated that F^- ion addition affected the (PO_4^{3-}) and P–O bonds which resulted in a hydrophilic HA structure [17]. OH…F bond gave a negative charge on the HA surface. Therefore, protein adsorption and cell attachment improved. Fathi and Zahrani studied the fluoridated HA synthesized by a mechanical alloying method [18] and observed some bands corresponding to (HPO_4^{2-}) ion [18]. It was also stated that (HPO_4^{2-}) ion could substitute with phosphate ions easily. Kannan et al. synthesized fluoride and chloride co-substituted HA, chlorapatite and fluorapatite by precipitation method and the samples were sintered at 900 °C for 2 h [15]. According to FTIR results, HA related bands were observed for only dried (not sintered) samples. In the samples of chlorapatite and fluorapatite, no (OH^-) related bands were observed as expected [15]. In another study ZnO nanopowders were investigated by FTIR spectroscopy [19] and, Zn–O symmetrical stretching band was observed in triaqua(1,10-phenanthroline-k^{2}N,N′)(sulfato-kO)zinc(II) which is abbreviated as (TPZS) with the formula of ($ZnSO_4(C_{12}H_8N_2)(H_2O)_3$) [20].

In the present study, Zn^{2+} and F^- ions were co-doped into HA structure by changing F^- amount. A detailed FTIR spectroscopic analysis of Zn^{2+} and/or F^- doped HA structure was performed for the first time. Samples were synthesized by precipitation method and sintered at 1100 °C for 1 h. Presence of phases in the samples was determined by X-ray diffraction (XRD) method. Moreover, besides the presentation of the observed bands, the differences between the concentrations with addition of ions were introduced by calculation of the area under the FTIR spectral bands related to the ion addition.

2. Experimental

Precipitation method was used to produce pure HA samples [21,22]. The precursors for this method were calcium nitrate tetrahydrate ($Ca(NO_3)_2 \cdot 4H_2O$) and diammonium hydrogen phosphate ($(NH_4)_2HPO_4$) obtained from Merck, Germany. These two powders were dissolved separately in distilled water with different amounts to obtain a theoretical Ca/P ratio of 1.67 and were stirred for 1 h. At the end of 1 h stirring, some ammonia solution (NH_4OH, (Merck, Germany)) was added to the solution with $(NH_4)_2HPO_4$. Then, Ca $(NO_3)_2 \cdot 4H_2O$ solution and some ammonia solution were added dropwise to adjust the pH level between 11 and 12. The final mixture was heated until it was boiled to speed up the reaction and the boiled mixture was left for stirring overnight. After 1 day of aging, this mixture was filtered and a wet cake was obtained. The wet cake was dried overnight at 200 °C to remove excess water and ammonia. The dried samples were sintered at 1100 °C for 1 h. In addition to precursors of Ca $(NO_3)_2 \cdot 4H_2O$ and $(NH_4)_2HPO_4$, zinc nitrate hexahydrate (Zn $(NO_3)_2 \cdot 6H_2O$) for Zn^{2+} doped samples and ammonium fluoride (NH_4F) for F^- doped samples were used. Table 1 summarizes the amounts of doping in terms of mole percentage for all samples.

The phases present in the samples were observed by XRD analysis by a Rigaku DMAX 2200 device and the percentage of the phases was detected by Rietvelt refinement analysis by using GSAS (The General Structural Analysis System) computer program. Cu-Kα radiation at 40 kV/40 mA was used for XRD analysis. The samples were scanned from 20° to 60° in 2θ with a scanning step size of 2.0°/min. To compare the positions of diffracted planes, Joint Committee on Powder Diffraction Standards (JCPDS) files were used.

FTIR spectroscopic technique was used to identify the presence of bonds formed in the pure and doped HA structures [23–26]. The samples were first crushed with a mortar and pestle. Then, the prepared powders were mixed with extensively dried potassium bromide (KBr) with 1 to 100 weight ratio. The prepared powder mixtures were dried in vacuum by freeze drying for 1 day. Then, the samples were cold pressed for 8 min to obtain transparent pellets. The spectra were recorded from 4000 cm^{-1} to 400 cm^{-1} using a 100 scan on Spectrum One Spectrometer (Perkin Elmer, Norwalk, CT, USA). In order to be sure that there is no variation due to the sample thickness, three different spectra were collected

Table 1
Naming, percentages of doping by mole and Ca/P ratio for prepared samples.

Sample ID	Zn^{2+} (mol%)	F^- (mol%)	Ca/P
Pure	–	0	1.67
2Zn	2	0	1.63
1F	–	1	1.67
2.5F	–	2.5	1.67
5F	–	5	1.67
2Zn1F	2	1	1.63
2Zn2.5F	2	2.5	1.63
2Zn5F	2	5	1.63

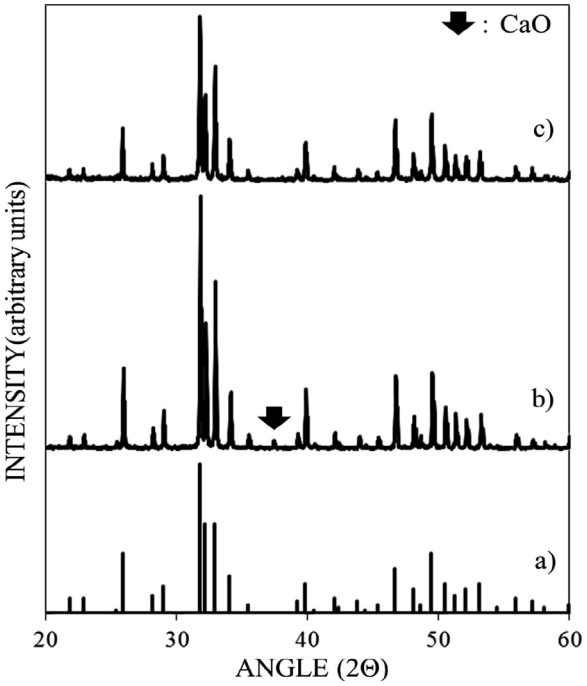

Fig. 1. X-ray diffraction patterns of (a) HA Reference (JCPDS#: 9-432), (b) pure HA, and (c) 5F.

from the different pellets belonging to same sample and checked that they were identical. The average of these three spectra was then used for further studies. For each experimental group, three independent samples were prepared and their average FTIR spectra values were compared with each other. For the analysis of infrared spectral data, Perkin Elmer Spectrum One software package was used. Statistical analysis of FTIR studies were done by using Minitab Statistical Software, USA. Paired t test was applied to the samples and $p < 0.05$ was accepted as a significant difference.

3. Results and discussion

XRD results of the samples pure HA and 5F are presented in Fig. 1. According to Fig. 1, all samples showed the same pattern with HA reference pattern that was obtained from Standard HA (JCPDS#: 9-432) [4]. The samples 2Zn1F, 2Zn2.5F and 2Zn5F had the XRD spectra similar to XRD spectra of 5F which did not contain any additional phase ("c" in Fig. 1). However, the samples 2Zn, 1F and 2.5F had XRD spectra similar to XRD spectra of pure HA which contained an additional peak that corresponded to the CaO phase ("b" in Fig. 1). CaO phase was formed by the incorporation of Zn^{2+} ions into HA hexagonal structure [27]. When Zn^{2+} ion replaced Ca^{2+} ion in HA, Ca^{2+} ions detached from HA structure to form CaO. Therefore, it may be the reason of CaO presence in the samples doped with Zn^{2+} ions. When XRD spectra of fluoridated samples were investigated, it can be said that CaO phase disappeared in 5F and Zn^{2+} and F^- co-doped samples. It is due to the fact that F^- makes the HA structure more stable. Therefore, presence of other phases was inhibited. Co-doping of Zn^{2+} and F^- ions resulted in further increase in stability of HA.

A detailed FTIR spectroscopic analysis was applied to the samples to observe the changes with F^- and Zn^{2+} addition separately and together by comparing with pure HA as the control. Changes in the spectra of doped samples when compared with pure HA spectra were the indicator of successful incorporation of the Zn^{2+} and F^- ions into the HA structure.

FTIR absorbance spectra for pure HA in 4000–400 cm^{-1} region is presented in Fig. 2. The peaks specific to HA structure are seen in this spectra. Moreover, the peaks assigned in HA absorbance spectra are seen in Table 2. The band corresponding to the functional group of (PO_4^{3-}) with vibrational mode of ν_1 was observed at 960 cm^{-1}. Moreover, other vibrational modes of (PO_4^{3-}) functional group were observed at 473 cm^{-1} for ν_2, 1045 and 1091 cm^{-1} for ν_3, 568 and 601 cm^{-1} for ν_4, respectively. Functional groups of (OH^-) were observed in two different modes which were librational mode at 632 cm^{-1} and stretching mode at 3571 cm^{-1}, respectively.

Fig. 3A shows the FTIR absorbance spectra for pure HA and F^- and/or Zn^{2+} doped samples in 3600–3320 cm^{-1} region. The band observed at 3571 cm^{-1} in pure HA spectra is assigned to the stretching vibration of the structural (OH^-). By the addition of 2 mol% Zn^{2+} into HA, the band shifted to 3570 cm^{-1} [11,13–15,17]. Moreover, 1 mol % addition of F^- ion resulted in a shift to 3570 cm^{-1}. As the amount of F^- increased in the samples, the bands gradually shifted to the smaller wavenumbers (it became 3569 cm^{-1} for 2.5F and 3567 cm^{-1} for 5F, respectively). Zn^{2+} and F^- doped samples followed the same trend as F^- doped samples followed. The shifts in the absorptions are indicator of changes in structure, conformation and intermolecular interaction [28]. In this study, the wavenumbers decreased with increasing F^- amount in band at 3571 cm^{-1}. The shifts in the wavenumbers of the band at 3571 cm^{-1} stemmed from the increase in number of hydrogen bonds between F^- ion and H atom of (OH^-) ion with F^- addition (Fig. 3A). Intensity of the peaks at 3571 cm^{-1} decreased with increasing F^- amount in the samples (Fig. 3A) [22]. This is due to the fact that F^- ion replaces the (OH^-) ion

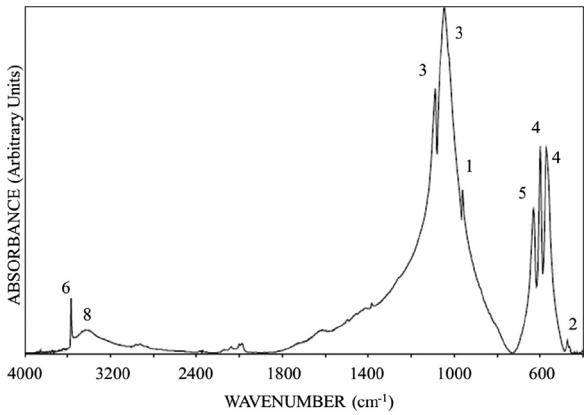

Fig. 2. FTIR absorbance spectra of pure HA in 4000–400 cm^{-1} region.

Table 2
Assignments of FTIR absorption bands of pure HA after sintering at 1100 °C for 1 h in 4000–400 cm^{-1} region [14,17–19].

Peak no.	Functional groups	Vibration mode	Wavenumber (cm^{-1})
1	$(PO_4)^{3-}$	ν_1	960
2	$(PO_4)^{3-}$	ν_2	473
3	$(PO_4)^{3-}$	ν_3	1045, 1091
4	$(PO_4)^{3-}$	ν_4	568, 601
5	OH^-	Librational	632
6	OH^-	Stretching	3571
7	OH…F		711, 354
8	Zn–O	Stretching	3403, 433

in the structure of HA. As the F^- amount in the samples increased, the concentration of (OH^-) ion in the structure of HA decreased due to the replacement with F^- ion which resulted in a decrease in the intensity of the peaks at 3571 cm^{-1} [29]. This was the indicator of successful incorporation of F^- ion into the structure of HA. Differences in the intensities and the area under the bands were strongly related with the concentration of the functional groups [30,31]. Therefore, area under the peak at 3571 cm^{-1} was also calculated for all samples and the results were represented in Fig. 4A. This figure showed that there is a statistical difference between pure HA, 2.5F, and 5F, and in between 2.5F and 5F. Moreover, 2Zn5F sample had significantly lower (OH^-) band area at 3571 cm^{-1} than that of the pure HA, 2Zn1F and 2Zn2.5F samples. This indicates that the concentration of (OH^-) functional group decreased in the sample 2Zn5F due to the replacement of F^- group with (OH^-) group [30,31]. The changes in the area under the peak at 3571 cm^{-1} suggested that F^- ion addition with the amounts of 1 mol%, 2.5 mol% and 5 mol% was succeeded.

Another important band in F^- doped samples is at 3543 cm^{-1}. This band corresponds to the bond OH…F. Therefore, this band was only seen in F^- doped samples. A small shift was seen in sample of 5F (at 3542 cm^{-1}). A relatively high amount of shift was observed for 2Zn5F (at 3538 cm^{-1}). The shifts to the lower wavenumbers with addition of F^- ion are also related with an increase in the number of hydrogen bonds between F^- ion and H atom in (OH^-) ion [29,30]. As the F^- amount increased in the HA structure, the number of hydrogen bonds between F^- ion and H atom in (OH^-) ion increased which resulted in a decrease in wavenumbers of the band at 3543 cm^{-1} (Fig. 3A) [30,31]. Moreover, in Fig. 3A, samples without F^- ion (Pure HA and 2Zn) do not have any bands at 3543 cm^{-1} as expected. The band at 3543 cm^{-1} is the evidence of the successful incorporation of F^- ion into the structure of HA.

The area under the band at 3543 cm^{-1} was also calculated for F^- doped samples. Fig. 4B represents the area under the band which corresponds to the OH…F bond. According to Fig. 4B, the area under the band at 3543 cm^{-1} increased with F^- amount in the samples. The increase in the area becomes significant for the sample of 5F when comparing with 1F and

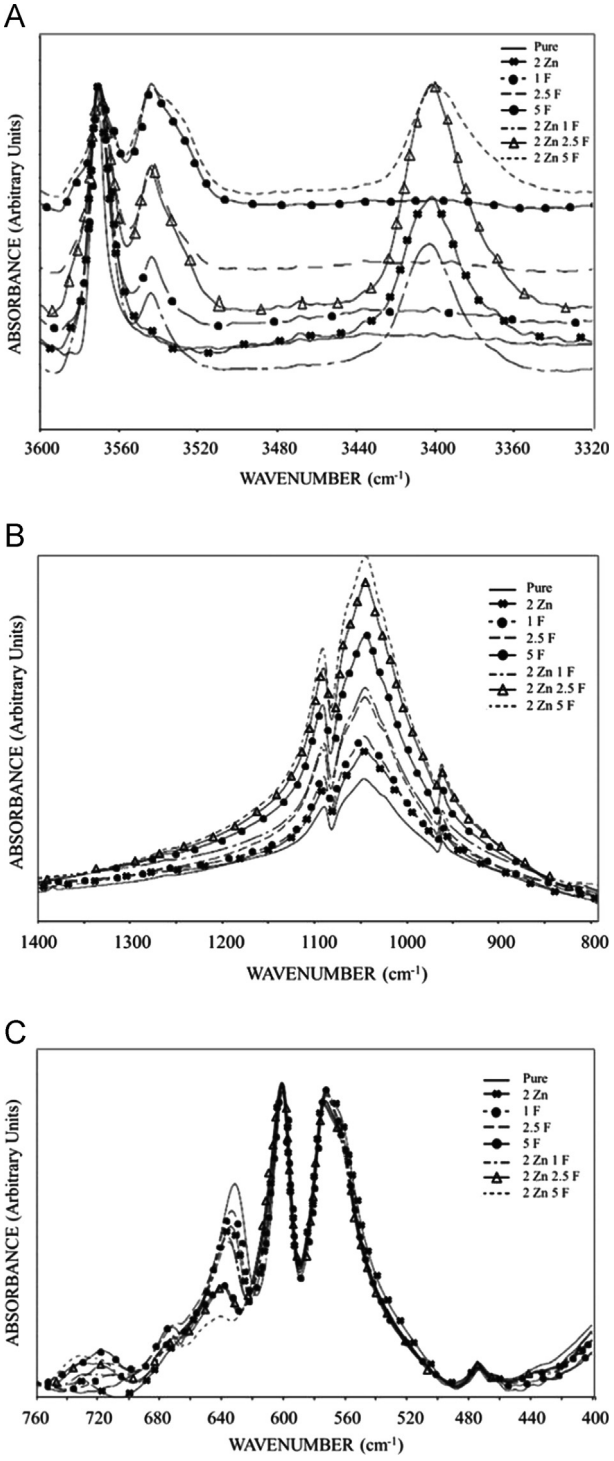

Fig. 3. FTIR absorbance spectra of pure HA, F^- and/or Zn^{2+} doped samples (A) in 3600–3320 cm^{-1} region. (Normalization was done with respect to the band at 3575 cm^{-1}), (B) in 1400–800 cm^{-1} region. (Normalization was done with respect to the band at 2820 cm^{-1}), (C) in 760–400 cm^{-1} region. (Normalization was done with respect to the band at 490 cm^{-1}).

2.5F. For the samples doped with Zn^{2+} and F^- ions, a significant increase is seen between 2Zn1F and 2 Zn2.5F, and between 2Zn2.5F and 2Zn5F. The difference in the area under the band at 3543 cm^{-1} is the evidence of successful

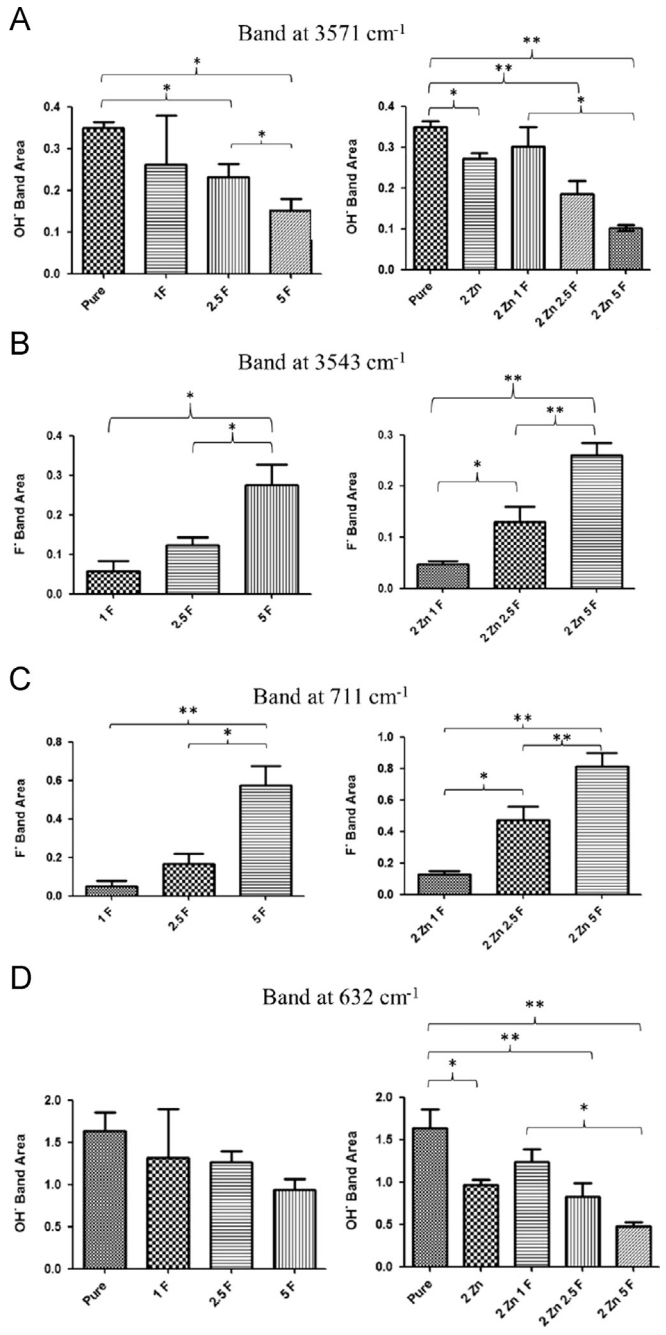

Fig. 4. (A) The OH^- stretching band area at 3570 cm^{-1} for pure and Zn^{2+} and/or F^- doped samples, (B) The OH…F band area at 3543 cm^{-1} for pure and Zn^{2+} and/or F^- doped samples, (C) The OH…F band area at 711 cm^{-1} for pure and Zn^{2+} and/or F^- doped samples, (D) The OH^- librational and area at 632 cm^{-1} for Pure and Zn^{2+} and/or F^- doped samples (* denotes $p < 0.05$ and ** denotes $p < 0.01$).

incorporation of F^- ion into the HA structure with the ion amounts of 1 mol%, 2.5 mol% and 5 mol%.

In Fig. 3A, the band at 3403 cm^{-1} is seen only in Zn^{2+} doped samples. Therefore, this band was assigned to the Zn–O symmetrical stretching. F^- doping resulted in a shift to the smaller wavenumbers in Zn–O symmetrical stretching band. The band at 3403 cm^{-1} is the indicator of successful incorporation of Zn^{2+} ion into the HA structure.

F^- addition resulted in small shifts to the higher wavenumbers at bands 1091 and 1045 cm^{-1}. However, no significant change was observed for the band at 960 cm^{-1} (Fig. 3B). Moreover, the intensities and the areas under these three bands did not change with Zn^{2+} and/or F^- addition. However, for the samples of Pure HA and 2Zn, there are some differences in the area under the bands at 1091, 1045 and 960 cm^{-1}. There is a significant decrease in the area under these (PO_4^{3-}) related bands in 2Zn spectra when compared with those in pure HA spectra. This is due to the fact that some Zn^{2+} ions may replace with P^{5+} ions in the (PO_4^{3-}) or may distort P^{5+} ions and break the bonds between P^{5+} and O^{2-}.

The bands between the wavenumbers of 711 and 727 cm^{-1} correspond to the bond OH…F. The band at 711 cm^{-1} shifted to an higher wavenumber with F^- and Zn^{2+} addition. In Fig. 3C, the bands at between 711 and 727 cm^{-1} can be seen clearly. Shifts in wavenumbers to the low frequencies can be interpreted as the increase in the strength of hydrogen bonds in the structure and increase in bond formation in the structure [32,33]. However, for the band at 711 cm^{-1}, there was an increase in wavenumbers by Zn^{2+} and F^- addition which is inconsistent with other F^- and (OH^-) related bands.

The area under the band at 711 cm^{-1} was also calculated for F^- doped samples. The results were represented in Fig. 4C. According to Fig. 4C, there is an increase in the area under the band at 711 cm^{-1} as a result of F^- addition. Significant increase is seen between the samples 1F and 5F, and also 2.5F and 5F. In F^- and Zn^{2+} doped samples, the changes in the area values are significant for all samples [12]. The increase in the area under the band at 711 cm^{-1} is indicator of an increase in the concentration of F^- functional group in HA structure [31,34]. Like the band at 3543 cm^{-1}, the band at 711 cm^{-1} is the indicator of successful addition of F^- ion into the HA structure.

The band at 632 cm^{-1} corresponding to (OH^-) librational mode was shifted to 635 cm^{-1} by 2 mol% Zn^{2+} addition [15]. F^- ion doping also increased the wavenumber of the pure HA. The increase in wavenumber with F^- ion amount was also seen in F^- and Zn^{2+} doped samples. The shifts to higher wavenumbers with F^- and Zn^{2+} ion addition at 632 cm^{-1} band show inconsistent pattern with the OH…F and (OH^-) stretching bands observed between 3600 cm^{-1} and 3403 cm^{-1} [32,33].

In Fig. 4D, although a decrease in (OH^-) librational band area with F^- addition is observed, changes in the areas do not have significant meanings. However, when Zn^{2+} ion is incorporated into the HA structure, it results in significant changes in the areas under the band at 632 cm^{-1}. The decrease in the band areas at 632 cm^{-1} with F^- addition is seen in F^- and Zn^{2+} co-doped samples in Fig. 4D. Comparing with (OH^-) stretching band, (OH^-) librational band was affected less by F^- addition.

No significant difference in the wavenumbers was detected for the bands at 601 and 568cm^{-1} which corresponded to (PO_4^{3-}) with vibrational mode of ν_4. Another band related with (PO_4^{3-}) group was detected at 473 cm^{-1} which corresponded to the vibrational mode of ν_2 [19]. There was not any significant shift

for the band at 473 cm^{-1} (Fig. 3C). The bands at 601, 568 and 473 cm^{-1} have nearly the same intensities in all samples. This is an indicator of the fact that Zn^{2+} and F^- addition did not affect these (PO_4^{3-}) related bands. These three bands at 601, 568 and 473 cm^{-1} are also the evidence of formation of HA structure with the solution precipitation method.

There was a small band at 433 cm^{-1} in Zn^{2+} containing samples (Fig. 3C) [20]. Therefore, this band was assigned to Zn–O symmetrical stretching band. Insignificant fluctuations between Zn^{2+} doped samples were seen around this band.

4. Conclusion

Pure HA, Zn^{2+} and/or F^- doped HA samples were synthesized by precipitation method. XRD results showed that HA and trace amount of CaO phase were detected in all samples except for Zn^{2+} and F^- co-doped samples and 5F sample. The intensity of CaO phase increased when Ca^{2+} ion introduced to the system was increased. (PO_4^{3-}) related bands detected at 1091, 1045, 960, 601, 568 and 473 cm^{-1} and (OH^-) related bands detected at 632 (librational) and 3571 (stretching) cm^{-1} are the indicator of the fact that HA synthesis was successful. Moreover, the bands at 3543 and 711 cm^{-1} were detected in F^- doped samples. The detection of these bands showed the fact that F^- ion was accepted by the structure of HA. The decrease in the intensities and/or areas of the (OH^-) related bands with the F^- ion addition showed that (OH^-) ion replaced with F^- ions. Furthermore, the bands at 3403 and 433 cm^{-1} were detected only in Zn^{2+} doped samples. This situation showed that Zn^{2+} was incorporated into the HA structure successfully. The results also showed that Zn^{2+} and F^- ions can be incorporated to HA structure successfully. HA gains different mechanical and biological properties according to the amount of addition and type of these ions. Therefore, detection of the amount of these ions in the HA structure by FTIR spectroscopy was important in terms of monitoring the differences in mechanical and biological properties of HA by ion addition.

References

[1] S.C. Cowin, Bone Mechanics, CRC Press, Boca Raton, FL, USA, 1989.

[2] B. Wopenka, J.D. Pasteris, A mineralogical perspective on the apatite in bone, Materials Science and Engineering C 25 (2005) 131–143.

[3] M.C.F. Magalhaes, P.A. Williams, Apatite group minerals: solubility and environmental remediation, in: T.M. Letcher (Ed.), Thermodynamics, Solubility and Environmental Issues, Elsevier B.V., Oxford, UK, 2007, pp. 327–342.

[4] Joint Committee on Powder Diffractions Standard (JCPDS) Database, Rigaku Qualitative Analysis ICDD (The International Centre for Diffraction Data) Software.

[5] S.L. Hall, H.P. Dimai, J.R. Farley, Effects of zinc on human skeletal alkaline phosphatase activity in vitro, Calcified Tissue International 64 (1999) 163–172.

[6] A. Peretz, T.E. Papadopoulos, D. Wiltems, A. Hotimsky, N. Michiels, M. Siderova, P. Bergmann, J. Neve, Zinc supplementation increases bone alkaline phosphatase in healthy men, Journal of Trace Elements in Medicine and Biology 15 (2001) 175–178.

[7] H.-W. Kim, Y.-J. Noh, Y.-H. Koh, H.-E. Kim, Enhanced performance of fluorine substituted hydroxyapatite composites for hard tissue engineering, Journal of Materials Science: Materials in Medicine 14 (2003) 899–904.

[8] M. Mousny, S. Omelon, L. Wise, E.T. Everett, M. Dumitriu, D. P. Holmyard, X. Banse, J.P. Devogelaer, M.D. Grynpas, Fluoride effects on bone formation and mineralization are influenced by genetics, Bone 43 (2008) 1067–1074.

[9] M.A. Rauschmann, T.A. Wichelhaus, V. Stirnal, E. Dingeldein, L. Zichner, R. Schnettler, V. Alt, Nanocrystalline hydroxyapatite and calcium sulphate as biodegradable composite carrier material for local delivery of antibiotics in bone infections, Biomaterials 26 (2005) 2677–2684.

[10] S. Catros, F. Guillemot, E. Lebraud, C. Chanseau, S. Perez, R. Bareille, J. Amédée, J.C. Fricain, Physico-chemical and biological properties of a nano-hydroxyapatite powder synthesized at room temperature, Ingenierie et Recherche Biomedicale 31 (2010) 226–233.

[11] A. Bianco, I. Cacciotti, M. Lombardi, L. Montanaro, E. Bemporad, M. Sebastiani, F-substituted hydroxyapatite nanopowders: thermal stability, sintering behaviour and mechanical properties, Ceramics International 36 (2010) 313–322.

[12] F. Freund, R.M. Knobel, Distribution of fluorine in hydroxyapatite studied by infrared spectroscopy, Journal of the Chemical Society 6 (1977) 1136–1140.

[13] A. Slosarczyk, Z. Paszkiewicz, C. Paluszkiewicz, FTIR and XRD evaluation of carbonated hydroxyapatite powders synthesized by wet methods, Journal of Molecular Structure 744–747 (2005) 657–661.

[14] S. Kannan, A. Rebelo, A.F. Lemos, A. Barba, J.M.F. Ferreira, Synthesis and mechanical behaviour of chlorapatite and chlorapatite/β-TCP composites, Journal of the European Ceramic Society 27 (2007) 2287–2294.

[15] S. Kannan, A. Rebelo, J.M.F. Ferreira, Novel synthesis and structural characterization of fluorine and chlorine co-substituted hydroxyapatites, Journal of Inorganic Biochemistry 100 (2006) 1692–1697.

[16] S.J. Kim, H.G. Bang, J.H. Song, S.Y. Park, Effect of fluoride additive on the mechanical properties of hydroxyapatite/alumina composites, Ceramics International 35 (2009) 1647–1650.

[17] H.U. Lee, Y.S. Jeong, S.Y. Park, S.Y. Jeong, H.G. Kim, C.R. Cho, Surface properties and cell response of fluoridated hydroxyapatite/TiO_2 coated on Ti substrate, Current Applied Physics 9 (2009) 528–533.

[18] M.H. Fathi, E.M. Zahrani, Mechanical alloying synthesis and bioactivity evaluation of nanocrystalline fluoridated hydroxyapatite, Journal of Alloys and Compounds 475 (2009) 408–414.

[19] Y.J. Kwon, K.H. Kim, C.S. Lim, K.B. Shim, Characterization of ZnO nanopowders synthesized by the polymerized complex method via an organochemical route, Journal of Ceramic Processing Research 3 (2002) 146–149.

[20] H. Ramesh, K. Parthipan, P.S. Rao, EPR, FTIR, powder XRD and optical absorption studies of Cu(II) ion in triaqua(1,10-phenanthroline-k2 N,N′)(sulfato-kO)zinc(II), Applied Magnetic Resonance 40 (2011) 513–524.

[21] Z. Evis, Al^{3+} doped nano-hydroxyapatites and their sintering characteristics, Journal of the Ceramic Society of Japan 114 (2006) 1001–1004.

[22] S.M. Toker, A. Tezcaner, Z. Evis, Microstructure, microhardness, and biocompatibility characteristics of yttrium hydroxyapatite doped with fluoride, Journal of Biomedical Materials Research Part B: Applied Biomaterials 96 (2011) 207–217.

[23] I. Rehman, W. Bonfield, Characterization of hydroxyapatite and carbonated apatite by photo acoustic FTIR spectroscopy, Journal of Materials Science: Materials in Medicine 8 (1997) 1–4.

[24] C.J. Liao, F.H. Lin, K.S. Chen, J.S. Sun, Thermal decomposition and reconstitution of hydroxyapatite in air atmosphere, Biomaterials 20 (1999) 1807–1813.

[25] M. Sivakumar, T.S.S. Kumar, K.L. Shantha, K.P. Rao, Development of hydroxyapatite derived from Indian coral, Biomaterials 17 (1996) 1709–1714.

[26] A. Rapacz-Kmita, C. Paluszkiewicz, A. Slosarczyk, Z. Paszkiewicz, FTIR and XRD investigations on the thermal stability of hydroxyapatite during hot pressing and pressureless sintering processes, Journal of Molecular Structure 744 (2005) 653–656.

[27] Z. Evis, Microstructural investigation of Cu^{2+} doped nano-hydroxyapatites, Materials Science and Technology 26 (2010) 630–632.
[28] G. Cakmak, I. Togan, F. Severcan, 17β-estradiol induced compositional, structural and functional changes on rainbow trout liver, revealed by FTIR spectroscopy: a comparative study with nonylphenol, Aquatic Toxicology 77 (2006) 53–63.
[29] N.S. Ozek, S. Tuna, A.E. Erson-Bensan, F. Severcan, Characterization of microRNA-125b expression in MCF7 breast cancer cells by ATR-FTIR spectroscopy, Analyst 135 (2010) 3094–3102.
[30] A. Dogan, G. Siyakus, F. Severcan, FTIR spectroscopic characterization of irradiated hazelnut (*Corylus avellana* L.), Food Chemistry 100 (2007) 1106–1114.
[31] S. Garip, F. Bozoglu, F. Severcan, Differentiation of mesophilic and thermophilic bacteria with FTIR spectroscopy, Applied Spectroscopy 61 (2007) 186–192.
[32] S. Garip, A.C. Gozen, F. Severcan, Use of Fourier transform infrared spectroscopy for rapid comparative analysis of Bacillus and Micrococcus isolates, Food Chemistry 113 (2009) 1301–1307.
[33] Infrared Spectroscopy, http://www.umsl.edu/~orglab/documents/IR/IR2.html.
[34] J. Kneipp, M. Beekes, P. Lasch, D. Naumann, Molecular changes of preclinical scrapie can be detected by infrared spectroscopy, The Journal of Neuroscience 22 (2002) 2989–2997.